

Microenergy Harvesters Based on Fluorinated Ethylene Propylene Piezotubes

Sergey Zhukov, Heinz von Seggern,* Xiaoqing Zhang, Yuan Xue, Omar Ben Dali, Perceval Pondrom, Gerhard M. Sessler, and Mario Kupnik

Energy harvesting from vibrations provides power to low-energy-consuming electronics for standalone and wearable devices as well as for wireless and remote sensing. In this contribution, compact tubular ferroelectric energy harvesters utilizing a single-tube design are presented. Such single-tube harvesters can be fabricated from commercially available fluorinated ethylene propylene (FEP) tubes with wall thicknesses of 25 and 50 μm , respectively, by mechanical deformation at elevated temperature. It is demonstrated that the generated power is highly dependent on parameters such as wall thickness, load resistance, and seismic mass. Utilizing a seismic mass of 80 g at resonance frequencies around 80 Hz and an input acceleration of $1 \times g$ (9.81 m s^{-2} rms), output powers up to 300 μW can be reached for a transducer with 25 μm thick walls.

Vibrational energy harvesting using piezoelectric transducer mechanisms has long been based on piezoceramics such as lead zirconate titanate (PZT). However, with increasing restrictions on the use of toxic lead, alternatives to lead-based materials have to be investigated. This has stimulated an extensive research on lead-free piezoelectric materials in the form of ceramics^[5,6] as well as ferroelectric polymers such as polyvinylidene fluoride (PVDF) and its copolymers.^[7–11] The latter materials are advantageous to ceramics due to their high flexibility, excellent processability, low dielectric constant, and low acoustic impedance combined with low manufacturing costs. A disadvantage compared to piezoceramics is their lower efficiency due to a small piezoelectric d_{33} coefficient of $10\text{--}40 \text{ pC N}^{-1}$, which is more than an order of magnitude smaller than that of PZT ceramics.

1. Introduction

Nowadays the popularity of mobile electronic devices is undoubtedly growing. Currently, rechargeable batteries are used to power such devices. This charging presents problems in remote locations where no power supplies are available. Therefore, self-powered technologies from ambient sources commonly associated with energy harvesting from heat, light, and/or mechanical vibrations have to be utilized.^[1–4]


In contrast, ferroelectrets or piezoelectrets^[12,13] have been shown to exhibit significantly higher d_{33} coefficients in the range of $100\text{--}3000 \text{ pC N}^{-1}$ due to mechanically soft air voids embedded in a poled semirigid polymer framework.^[14–16] Several harvesting applications of such material composites have been demonstrated profiting from their very large piezoelectric d_{33} coefficients.^[17–26] Among them are cellular polypropylene (PP) devices whose generated power was originally about $1 \mu\text{W}$ for a harvester of an active area of about 1 cm^2 and a seismic mass of a few grams, for an extrapolated acceleration of $g = 9.81 \text{ m s}^{-2}$.^[17–21] Design optimization led in relatively short times to a significantly higher power output of more than $100 \mu\text{W}$ for somewhat larger masses.^[20] However, the disadvantage of PP is that the charge and therewith the piezoelectricity is thermally stable only up to $+60 \text{ }^\circ\text{C}$.^[13] Therefore, other voided polymers have been considered as well.^[22–28] Best results so far have been obtained with ferroelectret harvesters made of laminated films of fluorinated ethylene propylene (FEP) combining good thermal stability with high output power of up to $100 \mu\text{W}$ for seismic masses on the order of 0.1 g .^[28] Other promising substitutes to PP ferroelectrets with better thermal stability are polytetrafluoroethylene (PTFE) piezotubes^[29] and FEP tube arrays,^[30,31] where the latter exhibit promising d_{33} coefficients but have not been explored for energy harvesting applications yet.

Consequently, single air-filled FEP tubes as miniaturized polymer ferroelectret harvesters were investigated. Therefore, single FEP tubes were deformed at elevated temperatures, subsequently metallized on both sides, and then polarized in high

Dr. S. Zhukov, Prof. H. von Seggern
Institut für Materialwissenschaft
Technische Universität Darmstadt
Merckstrasse 25, 64283 Darmstadt, Germany
E-mail: seggern@e-mat.tu-darmstadt.de

Prof. X. Zhang, Dr. Y. Xue
Shanghai Key Laboratory of Special Artificial Microstructure Materials and Technology
School of Physics Science and Engineering
Tongji University
Siping Road 1239, 200092 Shanghai, China

O. Ben Dali, Dr. P. Pondrom, Prof. G. M. Sessler, Prof. M. Kupnik
Measurement and Sensor Technology
Technische Universität Darmstadt
Merckstrasse 25, 64283 Darmstadt, Germany

 The ORCID identification number(s) for the author(s) of this article can be found under <https://doi.org/10.1002/adem.201901399>.

© 2020 The Authors. Published by WILEY-VCH Verlag GmbH & Co. KGaA, Weinheim. This is an open access article under the terms of the Creative Commons Attribution License, which permits use, distribution and reproduction in any medium, provided the original work is properly cited.

DOI: 10.1002/adem.201901399

electric fields. For the determination of the power output they were exposed to mechanical vibrational stress in the thickness direction ([3–3] mode) at low frequencies (10 Hz to 1 kHz) utilizing a seismic mass. The power generated was determined as a function of the exciting frequency, seismic mass, and load resistance for two different FEP tubes with 25 and 50 μm thick walls, respectively. Experimental results were then compared with an existing analytical model and finally with the output powers obtained from harvesters with different geometrical structures.

2. Results and Discussion

Two commercial FEP tube types from ZEUS Ltd (USA) with equal diameters of 1 mm and wall thicknesses of 25 and 50 μm , respectively, were used for device fabrication. For the forming of a tube to a stadium-like cross section a 30 mm long piece of FEP tube was placed between two parallel metal plates and heated up to $+250^\circ\text{C}$ for 10 min. The distance between the plates was reduced gradually during heating until stabilized by two metallic spacers of calibrated thickness of 0.4 mm. **Figure 1** shows typical photomicrographs of such stadium-shaped cross sections of tubes with 25 and 50 μm thick walls, respectively. The shape was preserved at room temperature after removal of the plates. Electrical poling of the produced specimens was conducted by direct-contact charging in ambient air at room temperature. Therefore the tube was first metallized on the upper and lower flat areas with Al electrodes, as shown in **Figure 1c** (metallized area: $1\text{ mm} \times 20\text{ mm}$) and then charged by applying a bias voltage up to $\pm 6\text{ kV}$ from a high-voltage power supply HSN-35 (FUG GmbH) for a few seconds, sufficiently to fully charge the devices.^[31] It should be noted that the voltage V_{pol} at which the maximal residual polarization of the tubular structure is achieved can be approximately estimated as^[32–34]:

$$V_{\text{pol}} = 2 \times \left[d_{\text{air}} + \frac{2\varepsilon_{\text{air}}d_{\text{wall}}}{\varepsilon_{\text{wall}}} \right] E_{\text{B}} \quad (1)$$

where E_{B} corresponds to the threshold electric breakdown field strength in the air channel (Paschen's law),^[35] while d_{wall} and d_{air} denote the thickness of the wall and air channel with

corresponding relative dielectric permittivities of $\varepsilon_{\text{wall}}$ and ε_{air} , respectively. It must also be taken into account that the breakdown strength E_{B} in Equation (1) depends on d_{air} . For the present estimation, the values for E_{B} of 62 and 65 kV cm^{-1} were used for air gaps of 350 and 300 μm , respectively, while $\varepsilon_{\text{air}} = 1$ and $\varepsilon_{\text{wall}} = 2.1$. Under such conditions, Equation (1) delivers a value of 4.5 and 4.6 kV for the particular structures shown in **Figure 1a,b**, respectively.

After poling, the dynamic piezoelectric d_{33} responses of the obtained specimens were determined, as they represent one of the most important parameters of harvester devices. For measuring the dynamic d_{33} coefficient, the tubular sample and a seismic mass m_{s} placed on it were accelerated sinusoidally by a Bruel&Kjaer shaker. Thereby, the sample was loaded with two forces, namely the static force $m_{\text{s}} \times g$ and the dynamic force, $m_{\text{s}} \times a$, where a is the dynamic acceleration. The dynamic acceleration a was measured with an accelerometer in combination with a charge amplifier. Simultaneously, the charge Q generated by the tubular specimen in short circuit was measured by a second charge amplifier of the same model. In this way, the charge sensitivity S of the ferroelectret harvester could be determined as $9.81 \times Q_{\text{rms}}/a_{\text{rms}}$, where Q_{rms} and a_{rms} are the rms values of charge and dynamic acceleration.^[22] In addition, the dynamic piezoelectric coefficient can be calculated as $d_{33} = Q_{\text{rms}}/m_{\text{s}} \times a_{\text{rms}}$ for a fixed frequency significantly lower than the resonant frequency. In this work, the dynamic d_{33} coefficients were determined for a frequency of 20 Hz. More information about the measuring setup can be found in Section 4.

Exemplarily, the experimental results for simultaneously measured Q_{rms} and a_{rms} for a harvester fabricated from an FEP tube with 50 μm thick walls are shown in **Figure 2a,b** for various m_{s} , while the calculated charge sensitivities S for the same seismic masses are shown in **Figure 2c**. One can learn from **Figure 2c** that the tubular transducer displays remarkable and flat frequency responses for different m_{s} up to the resonance region located between 100 and 200 Hz. In addition, **Figure 2d** shows for the same harvester the dynamic d_{33} coefficients at the fixed frequency of 20 Hz as a function of seismic mass for a whole set of utilized m_{s} values and dynamic loads. It is remarkable that an increase in the dynamic mechanical load up to about 5 kPa does not weaken the piezoelectric response (see **Figure 2d**): the dynamic d_{33} coefficient stays constant at about 80 pC N^{-1} for seismic masses up to 180 g, which corresponds under the gravity of earth to a static pressure of 88 kPa. At the same time, the present experiments showed that a thin-walled sample has a noticeably higher dynamic response, $\approx 290\text{ pC N}^{-1}$, which, however, remains constant only up to $m_{\text{s}} = 80\text{ g}$. For a higher load, it begins to decrease remarkably. Based on these results, it can be concluded that a decrease in the thickness of the wall would lead to a significant increase in the dynamic piezoelectric response under low dynamic loads, and to a significant degradation under elevated mechanical loads.

The same experimental setup was used to measure the output power generated by tubular harvesters excited at various frequencies and load resistances R_{L} . The output power was obtained experimentally from the relation

$$P_{\text{out}} = R_{\text{L}} I^2 = R_{\text{L}} \omega^2 Q_{\text{R1,rms}}^2 \quad (2)$$

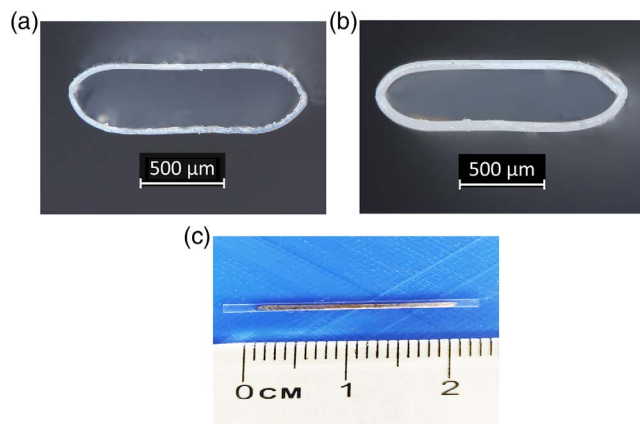


Figure 1. Cross-section micrographs of resulting stadium-like structures fabricated at $+250^\circ\text{C}$ from FEP tubes of diameter of 1 mm and with wall thicknesses of a) 25 and b) 50 μm . c) Dimensions of actual tube harvester.

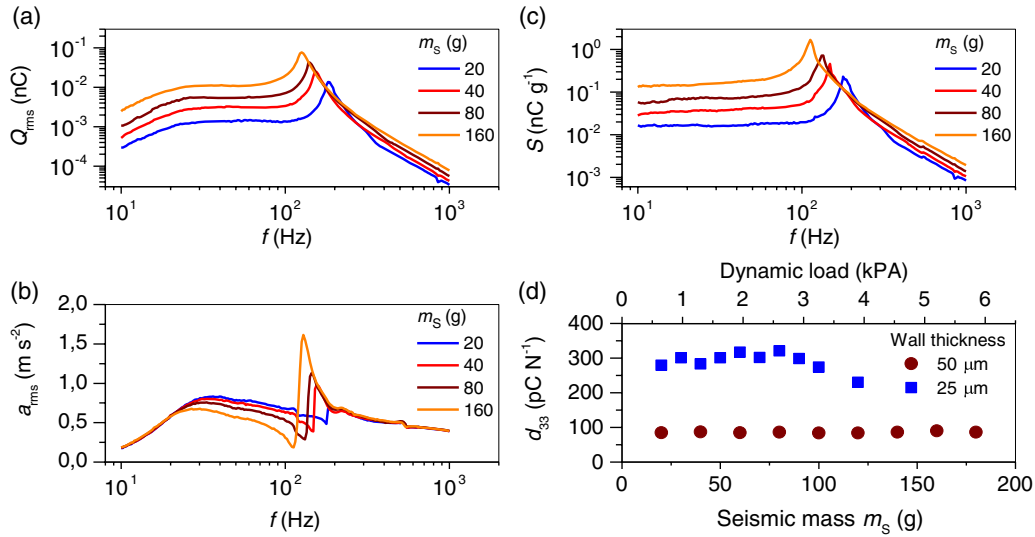


Figure 2. a) Charge Q_{rms} generated in short circuit by a single-tube transducer in response to an applied dynamic force $m_s \times a$ as a function of frequency. b) Acceleration a_{rms} and c) charge sensitivity S versus frequency for different seismic masses m_s as indicated. d) Dynamic d_{33} coefficient at 20 Hz versus seismic mass and corresponding dynamic load for transducers with different wall thickness as indicated.

where I and $Q_{R_L,rms}$ represent the current and charge (rms) through the load resistor, and ω represents the angular frequency of the shaker. The value P_N normalized to an acceleration of $g = 9.81 \text{ m s}^{-2}$ is then given by

$$P_N = P_{out} \left(\frac{g}{a_{rms}} \right)^2 \quad (3)$$

where a_{rms} is the measured acceleration.

Results of the output power P_N generated by a thick-walled ferroelectret harvester for $m_s = 60 \text{ g}$ and various load resistances R_L are shown in **Figure 3a** as a function of the vibrational frequency. The figure indicates that the output power increases with increasing frequency below the resonance frequency. A maximum value of $P_N = 20 \text{ } \mu\text{W}$ is obtained at the resonance frequency of 140 Hz and an optimum load resistance of $R_{opt} = 190 \text{ M}\Omega$ corresponding to a harvester capacity. $C_s = 6 \text{ pF}$. This is especially well seen in **Figure 3b**, which shows the peak output power P_N^{max} as a function of the load resistance. As expected, the output power increases at low resistance R_L proportional to R_L and decreases proportionally to $1/R_L$ for R_L much larger than the optimal load resistance R_{opt} .^[23] In the present case, the total harvester capacitance C_s is greater than the capacitance of the tubular transducer itself, which amounts to about 2 pF. This is understandable due to the relatively large parasitic capacitance between the seismic mass and the support plate compared to the actual transducer.

It was previously revealed that the normalized power output P_N generated by a ferroelectret harvester in a load resistance R_L in response to an input acceleration g at the circular frequency ω can be written as^[17,19]

$$P_N = \frac{R_L \omega^2 d_{33}^2 m_s^2 g^2}{\left[\left(\frac{\omega^2}{\omega_0^2} - 1 \right)^2 + 4\zeta^2 \left(\frac{\omega}{\omega_0} \right)^2 \right] + [1 + (R_L C_s \omega)^2]} \quad (4)$$

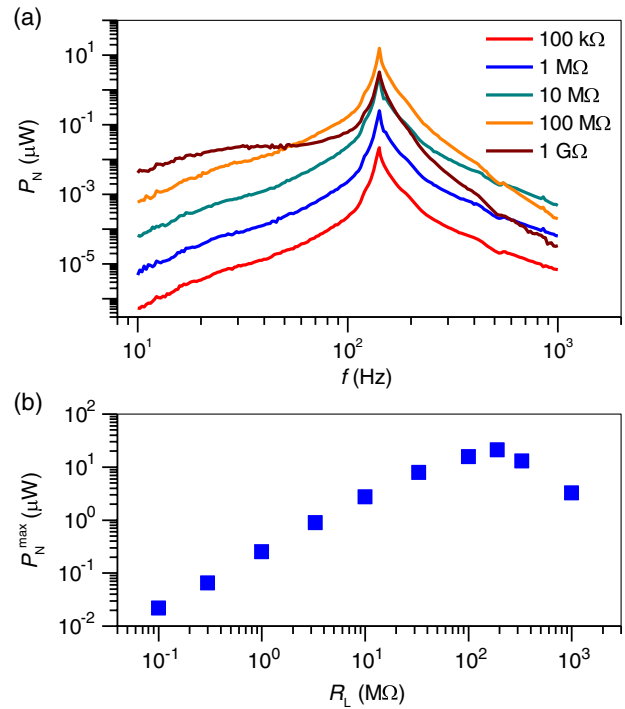


Figure 3. a) Output power P_N as a function of vibration frequency f for a single-tube FEP harvester (wall thickness $50 \text{ } \mu\text{m}$) at various load resistances R_L as indicated. b) Peak output power P_N^{max} as a function of load resistance R_L for the same harvester. The seismic mass m_s is 60 g.

where ω_0 is the resonance circular frequency of the harvester, C_s is the total harvester capacitance, consisting of the sum of the capacitance of the tubular transducer and the parasitic capacitance of the measuring setup, and $\zeta = \Delta\omega/2\omega_0$ is the damping ratio corresponding to half of the half-power bandwidth

$\Delta\omega/\omega_0$. According to Equation (4), the generated power is highly dependent on the seismic mass used. In addition, the normalized peak power P_N^{\max} generated in an optimal load resistance $R_{\text{opt}} = (C_s\omega_0)^{-1}$ can be expressed as^[17,19]

$$P_N^{\max} \cong \sqrt{\frac{YAm_s^3 d_{33}^2 g^2}{t 8\zeta^2 C_s}} \quad (5)$$

where Y is Young's modulus of a tubular harvester in the direction of compression, A the transducer area loaded by the seismic mass m_s , and t the total thickness of the device. According to Equation (5), P_N^{\max} is proportional to $m_s^{3/2}$. The latter dependence was experimentally verified for ferroelectret energy harvesters based on the longitudinal piezoelectric effect.^[17]

In this work, the influence of the seismic mass on the output power of tubular FEP harvesters was also investigated. **Figure 4a** shows the frequency dependence of P_N obtained for a thick-walled harvester at various seismic masses m_s for optimal load resistances. Two kinds of effects can be easily identified with increasing m_s . First of all, the normalized power output grows significantly for increasing seismic mass. As a result, the value of P_N^{\max} is enhanced from about $3 \mu\text{W}$ for $m_s = 20 \text{ g}$ to about $100 \mu\text{W}$ for $m_s = 160 \text{ g}$.

The second effect is the shift of the resonance maximum toward lower frequencies with increasing seismic mass. The experimentally obtained dependence of P_N^{\max} on m_s is shown in **Figure 4b**. A fit by the power-law function $P_N^{\max} = c \times m_s^b$, where c and b are the fitting parameters, results in

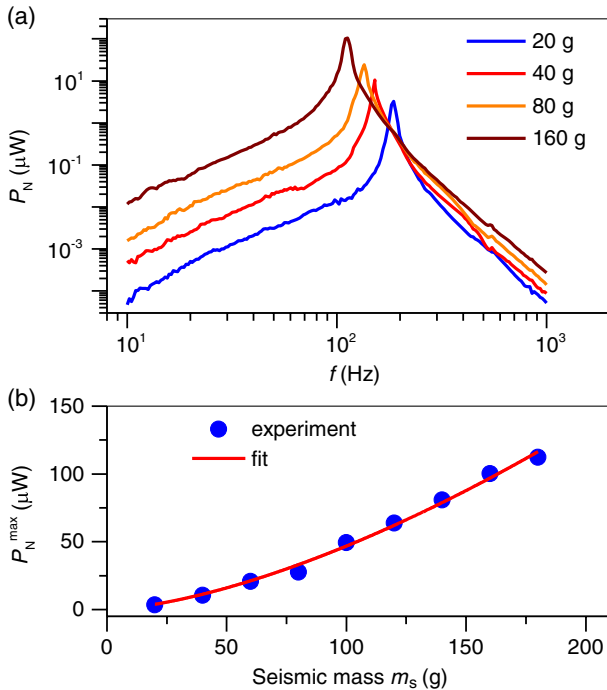


Figure 4. a) Output power P_N as a function of vibration frequency f for a single-tube FEP harvester (wall thickness $50 \mu\text{m}$) at various seismic masses m_s for an optimal load resistance. b) Peak output power P_N^{\max} as a function of m_s for an optimal load resistance. The symbols correspond to the experimental results, while the solid line represents the fit by the power function $P_N^{\max} = c \times m_s^b$.

$c = (3.73 \pm 1.29) \times 10^{-8} \text{ W g}^{-1}$ and $b = 1.55 \pm 0.07$ is also shown in **Figure 4b**. The value for parameter b agrees well with the expected mass dependence from Equation (5) where $P_N^{\max} \sim m_s^{3/2}$.

The output power P_N of a thin-walled tubular harvester (wall thickness of $25 \mu\text{m}$) as a function of vibrational frequency, load resistance, and seismic mass shows that the efficiency of harvesters is much higher, reaching P_N^{\max} values of about $300 \mu\text{W}$ for a seismic mass of 80 g . **Figure 5** compares the frequency responses of P_N for thin- and thick-walled harvesters under the same experimental conditions utilizing a seismic mass of 80 g and a load resistance of 330 and $190 \text{ M}\Omega$, respectively. It turned out that the peak output power of a thin-walled device is about one order of magnitude higher than that of the thick-walled specimen. Furthermore, the peak position of the generated power is shifted from about 135 Hz to a frequency of about 78 Hz for a thin-walled device, which is a clear advantage of such a harvester, as most of the energy from ambient mechanical vibrations is concentrated at very low frequencies.^[36]

In the next step, the experimental dependencies shown in **Figure 5** were fitted to Equation (4) utilizing the directly accessible parameters such as R_L , g , and m_s and experimentally determined values, such as the d_{33} constant (see **Figure 2d**) and the separately measured device capacitance C_s . The fit of Equation (4) then was used to determine the two variables ζ and ω_0 , which largely depend on the mechanical properties, the geometry of the sample, and the seismic mass. Both fit parameters are listed together with the other fixed parameters in **Table 1**. In these calculations, experimental values for the dynamic d_{33} , determined at 20 Hz , were used. C_s was measured separately using a capacitance meter. The obtained fits are also shown in **Figure 5** by dashed lines for both devices and agree very well with the experimental results.

The normalized power output of $100 \mu\text{W}$, generated with a seismic mass of around 100 g , falls in the range of generated powers of previously reported ferroelectret energy harvesters, e.g., based on cross-linked PP using the d_{33} effect.^[18–20] The power output related to the seismic mass is, however, still lower than that generated by thinner-walled FEP layered harvesters.^[28]

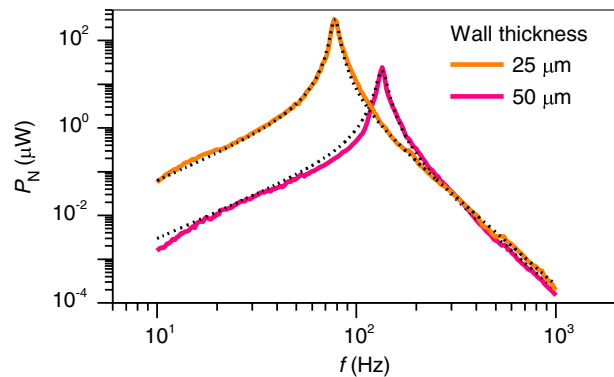


Figure 5. Comparison of the output power P_N for the energy harvesters based on single FEP tubes with different wall thicknesses as indicated. The solid lines represent the experimental results for the seismic mass of 80 g , while the dashed lines correspond to a fit using Equation (4) (see **Table 1**).

Table 1. Fitted and measured parameters for thin- and thick-walled tubular harvesters.

Wall thickness [μm]	R_L [$\text{M}\Omega$]	C_S [pF]	m_S [g]	d_{33} [pC N^{-1}]	ω_0 [rad s^{-1}]	f_0 [Hz]	ζ	Quality factor R^2
25	330	6	80	290	490 ± 1	78.1 ± 0.2	0.045 ± 0.002	0.994
50	190	6	80	80	845 ± 1	134.5 ± 0.2	0.058 ± 0.005	0.960

However, it has to be mentioned that in the present case the total capacitance C_S of the harvesters, including the parasitic capacitance, is in the range of 6 pF and therewith by a factor of at least 3 larger than the actual transducer capacitance. According to Equation (5), the generation of a far larger power can be expected if the parasitic capacitance is reduced. Another effective way to increase power output can be deduced from the comparison between thin- and thick-walled devices. Such a comparison clearly indicates that a further reduction of the wall thickness would drastically improve the power output.

Before concluding, it should be noted that the long-term stability of the developed harvesters is an important issue and depends on the temperature, humidity, and utilized mechanical load. It is known for ferroelectrets in general that their resistance to fatigue and aging is mainly determined by two factors: their mechanical and charge storage stability, where the latter is limited by the allowed temperature range. In the present case, the ferroelectrets are FEP-based and they have been shown to provide a lifetime at ambient temperature of up to 50 years and more.^[16,37–39] Concerning the mechanical stability, it has been demonstrated in this study that both thin- and thick-walled harvesters have certain limits for the applicable mechanical load. Under high loads, the tubular structures can partially collapse, which leads to the degradation of the piezoelectric response as shown in Figure 2d. Further investigation of device stability factors, such as the frequency dependence of the mechanical fatigue, influence of humidity and temperature, as

well as their not trivial interplay, need, however, more detailed research, which is beyond the scope of this work and will be published in an upcoming article.

3. Conclusions

In this work, compact ferroelectret energy harvesters of tubular design are introduced. These harvesters can be easily fabricated from commercially available FEP tubes with a wall thickness of 25 and 50 μm . With seismic masses of 20–180 g, the generation of power up to 300 μW at frequencies around 100 Hz is possible for an input acceleration of g (rms). It was experimentally verified that the power generated at the resonance frequency into the optimal load resistance is proportional to $m_S^{3/2}$. Energy harvesters based on the present design have several advantages: First, they are rather compact: without considering the volume of seismic mass used they have an active area of about 20 mm^2 and a height of 0.4 mm (see also Figure 1c). However, if necessary, the separate tubes can be fused or stacked together, forming an array with a much larger active area.^[30,31] Second, harvesters with seismic masses ranging from grams to kilograms can be realized by adjusting the wall thickness, suggesting that devices with thicker walls can withstand large mechanical loads.^[29] Third, the use of FEP as a base material ensures good temperature stability^[23,28,37–39] sufficient for most room temperature applications. The obtained experimental

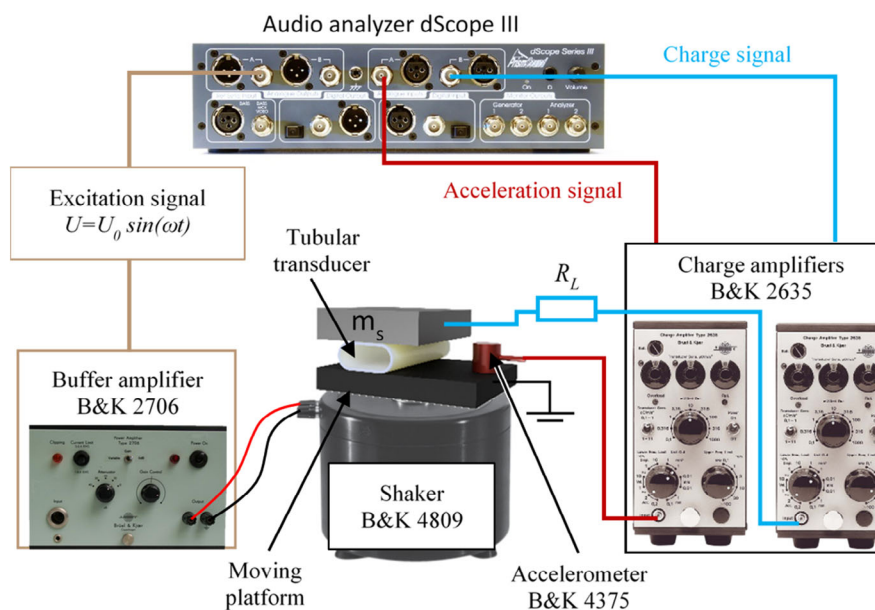


Figure 6. Schematic of experimental setup used for energy harvesting evaluation.

results are an excellent base for further optimizing the tube design, which can be used not only in vibration-based energy harvesters, but also in accelerometers.

4. Experimental Section

The experimental setup for characterizing the present ferroelectret energy harvesters is schematically shown in **Figure 6**. The setup included a seismic mass m_s placed on top of the tubular transducer, both mounted on a platform driven by an electrodynamic shaker (B&K 4809), which was fed by an audio analyzer (dScope Series III, PrismSound) through a buffer amplifier (B&K 2706). The harvester-generated current through a load resistor R_L was measured by a charge amplifier (B&K 2635) and rectified by the audio analyzer. In parallel, the acceleration was measured by an accelerometer (B&K 4393) mounted directly on the platform through a charge amplifier (B&K 2635) and the audio analyzer. Both signals were recorded at different frequencies for various load resistors and seismic masses and were used to calculate the frequency dependence of the output power. The same setup omitting the load resistor was used to measure the dynamic d_{33} coefficients.

Acknowledgements

This work was supported by the Deutsche Forschungsgemeinschaft (DFG) Grants Nr. SE 941/19-1 and SE 941/21-1, KU 3498/1-1 and the National Natural Science Foundation of China (NSFC) Grant Nr. 61761136004.

Conflict of Interest

The authors declare no conflict of interest.

Keywords

energy harvesting, ferroelectret generators, fluorinated ethylene propylene, piezoelectrets, piezotubes

Received: November 14, 2019

Revised: January 14, 2020

Published online: February 21, 2020

- [1] S. Priya, *J. Electroceramics* **2007**, *19*, 165.
 [2] P. D. Mitcheson, E. M. Yeatman, G. K. Rao, A. S. Holmes, T. C. Green, *Proc. IEEE* **2008**, *96*, 1457.
 [3] P. Basset, E. Blokhina, D. Galayko, *Electrostatic Kinetic Energy Harvesting*, John Wiley & Sons Inc, Hoboken, NJ **2016**.
 [4] N. Elvin, A. Erturk, *Advances in Energy Harvesting Methods*, Springer Science & Business Media, Berlin **2013**.
 [5] J. Rödel, W. Jo, K. T. P. Seifert, E.-M. Anton, T. Granzow, D. Damjanovic, *J. Am. Ceram. Soc.* **2009**, *92*, 1153.
 [6] S. Zhukov, M. Acosta, Y. A. Genenko, H. von Seggern, *J. Appl. Phys.* **2015**, *118*, 134104.
 [7] X. Chen, X. Han, Q.-D. Shen, *Adv. Electron. Mater.* **2017**, *3*, 1600460.
 [8] K. S. Ramadan, D. Sameoto, S. Evoy, *Smart Mater. Struct.* **2014**, *23*, 033001.
 [9] J. Schütrumpf, S. Zhukov, Y. A. Genenko, H. von Seggern, *J. Phys. D: Appl. Phys.* **2012**, *45*, 165301.
 [10] Y. M. Yousry, K. Yao, S. Chen, W. H. Liew, S. Ramakrishna, *Adv. Electron. Mater.* **2018**, *4*, 1700562.
 [11] F. Narita, M. Fox, *Adv. Eng. Mater.* **2018**, *20*, 1700743.
 [12] S. Bauer, R. Gerhard-Multhaupt, G. M. Sessler, *Phys. Today* **2004**, *57*, 37.
 [13] M. Paajanen, J. Leikkala, K. Kirjavainen, *Sens. Actuators A* **2000**, *84*, 95.
 [14] A. Mohebbi, F. Mighri, A. Ajji, D. Rodrigue, *Adv. Polym. Technol.* **2018**, *37*, 21686.
 [15] H. von Seggern, S. Zhukov, S. Fedosov, *IEEE Trans. Dielectr. Electr. Insul.* **2011**, *18*, 49.
 [16] X. Zhang, J. Hillenbrand, G. M. Sessler, S. Haberzettl, K. Lou, *Appl. Phys. A* **2012**, *107*, 621.
 [17] P. Pondrom, J. Hillenbrand, G. M. Sessler, J. Bös, T. Melz, *Appl. Phys. Lett.* **2014**, *104*, 172901.
 [18] S. R. Anton, K. M. Farinholt, A. Erturk, *J. Intell. Mater. Syst. Struct.* **2014**, *25*, 1681.
 [19] P. Pondrom, J. Hillenbrand, G. M. Sessler, J. Bös, T. Melz, *IEEE Trans. Dielectr. Electr. Insul.* **2015**, *22*, 1470.
 [20] X. Zhang, L. Wu, G. M. Sessler, *AIP Adv.* **2015**, *5*, 077185.
 [21] Z. Luo, D. Zhu, J. Shi, S. Beeby, C. Zhang, P. Proynov, B. Stark, *IEEE Trans. Dielectr. Electr. Insul.* **2015**, *22*, 1360.
 [22] P. Pondrom, G. M. Sessler, J. Bös, T. Melz, *Appl. Phys. Lett.* **2016**, *109*, 053906.
 [23] X. Zhang, G. M. Sessler, Y. Wang, *J. Appl. Phys.* **2014**, *116*, 074109.
 [24] Z. Luo, D. Zhu, S. Beeby, *Smart Mater. Struct.* **2016**, *25*, 045010.
 [25] B. Wang, J. Zhong, Q. Zhong, N. Wu, X. Cheng, W. Li, K. Liu, L. Huang, B. Hu, J. Zhou, *Adv. Electron. Mater.* **2016**, *2*, 1500408.
 [26] Y. Zhang, C. R. Bowen, S. K. Ghosh, D. Mandal, H. Khanbareh, M. Arafa, C. Wan, *Nano Energy* **2019**, *57*, 118.
 [27] X. Zhang, P. Pondrom, L. Wu, G. M. Sessler, *Appl. Phys. Lett.* **2016**, *108*, 193903.
 [28] X. Zhang, P. Pondrom, G. M. Sessler, X. Ma, *Nano Energy* **2018**, *50*, 52.
 [29] R. Kacprzyk, A. Mirkowska, *IEEE Trans. Dielectr. Electr. Insul.* **2018**, *25*, 759.
 [30] S. Zhukov, D. Eder-Goy, S. Fedosov, B.-X. Xu, H. von Seggern, *Sci. Rep.* **2018**, *8*, 4597.
 [31] S. Zhukov, D. Eder-Goy, C. Biethan, S. Fedosov, B.-X. Xu, H. von Seggern, *Smart Mater. Struct.* **2018**, *27*, 015010.
 [32] B.-X. Xu, H. von Seggern, S. Zhukov, D. Gross, *J. Appl. Phys.* **2013**, *114*, 094103.
 [33] S. Zhukov, H. von Seggern, *J. Appl. Phys.* **2007**, *102*, 044109.
 [34] S. Zhukov, S. Fedosov, H. von Seggern, *J. Phys. D: Appl. Phys.* **2011**, *44*, 105501.
 [35] Y. P. Raizer, *Gas Discharge Physics* (Ed. J. E. Allen), Springer, Berlin **1991**.
 [36] Y. Suzuki, *IEEE J Trans. Electr. Electron. Eng.* **2011**, *6*, 101.
 [37] H. von Seggern, S. Zhukov, S. Fedosov, *IEEE Trans. Dielectr. Electr. Insul.* **2010**, *17*, 1056.
 [38] H. von Seggern, J. E. West, *J. Appl. Phys.* **1984**, *55*, 2754.
 [39] H. von Seggern, *J. Appl. Phys.* **1979**, *50*, 7039.